Auditory Efferent System Modulates Mosquito Hearing

Marta Andrés[1†*], Marvin Seifert[1], Christian Spalthoff[1], Ben Warren[1#], Lukas Weiss[1,2], Diego Giraldo[1,2], Margret Winkler[1], Stephanie Pauls[1], and Martin C. Göpfert[1*]

[1]Department of Cellular Neurobiology, University of Göttingen, 37077 Göttingen, Germany.

[2]International Max Planck Research School Neurosciences, 37077 Göttingen, Germany

[†]Present address: Department for Infectious Disease Epidemiology, Robert Koch Institute, 13353 Berlin, Germany

[#]Present address: Department of Neuroscience Psychology and Behavior, University of Leicester, Leicester LE1 7RH, UK

*Correspondence: martaandresm@gmail.com (M.A.), mgoepfe@gwdg.de (M.C.G.)

Graphical abstract

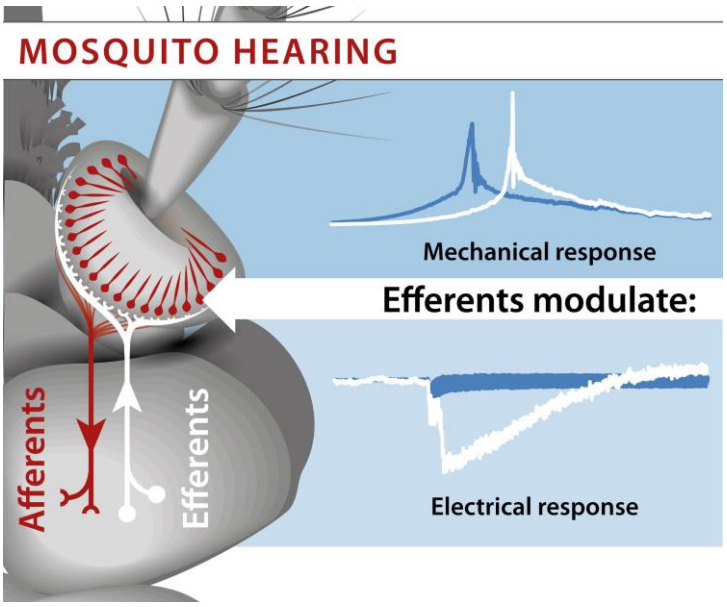

Highlights

- Auditory efferent systems analogous to those of vertebrates occur in mosquitoes
- Auditory efferents innervate dendrites and axons of auditory sensory neurons
- Efferent neurotransmitters/-modulators include octopamine, GABA, and serotonin
- Neurotransmitters/-modulators alter auditory organ performance

eTOC Blurb

Andrés *et al*. report that auditory efferent systems, as known from vertebrate hearing, modulate mosquito hearing organs.

Summary

The performance of vertebrate ears is controlled by auditory efferents that originate in the brain and innervate the ear, synapsing onto hair cell somata and auditory afferent fibers [1-3]. Efferent activity can provide protection from noise and facilitate the detection and discrimination of sound by modulating mechanical amplification by hair cells and transmitter release as well as auditory afferent action potential firing [1-3]. Insect auditory organs are thought to lack efferent control [4-7], but when we inspected mosquito ears we obtained evidence for its existence. Antibodies against synaptic proteins recognized rows of bouton-like puncta running along the dendrites and axons of mosquito auditory sensory neurons. Electron microscopy identified synaptic and non-synaptic sites of vesicle release, and some of the innervating fibers co-labelled with somata in the central nervous system (CNS). Octopamine, GABA, and serotonin were identified as efferent neurotransmitters/neuromodulators that affect auditory frequency tuning, mechanical amplification, and sound-evoked potentials. Mosquito brains thus modulate mosquito ears, extending the use of auditory efferent systems from vertebrates to invertebrates and adding new levels of complexity to mosquito sound detection and communication.

Results and discussion

Male mosquitoes rely on female wing-beat sounds to locate potential mates [8-11]. Sound detection is mediated by some 16,000 ciliated Johnston's organ (JO) neurons in the pedicel of each antenna [10, 12-14] (Fig. 1A). Analogous to vertebrate hair cells, JO neurons serve sensory and motor roles, transducing and amplifying sound-induced vibrations of the antennal flagellum [15-17]. Flagellar vibrations are transmitted to the circularly arranged neurons via

some 70 radial cuticular prongs [10,18] (Fig. 1A), and the neurons send axons into the brain where they synapse in the deutocerebrum [19]. This central synapsing means that there should be no peripheral synapses in JO, as was previously shown for *Drosophila melanogaster* [6]. When we labelled the JO of male *Culex quinquefasciatus* mosquitoes against the presynaptic protein SAP47 [20] (see Supplemental Experimental Procedures online), however, a punctate staining within JO was obtained (Fig. 1B). In longitudinal antennal sections, the anti-SAP47 antibody nc46 [20] recognized rows of puncta running through JO, and it also strongly labelled the proximal JO region where the axons of JO neurons come together to leave the pedicel (Fig. 1B). An equivalent staining was seen in oblique pedicellar sections (Supplemental Information online, Fig. S1A), including nc46 signals in the latter axonal region as well as rows of puncta running circularly through JO, peripherally to each prong. Inspection of confocal stacks revealed that, in longitudinal sections, nc46-positive fibers interconnect adjacent puncta (Fig. 1C), indicating that the puncta are associated with presynaptic fibers and represent synaptic boutons. Judged from oblique sections (Fig. S1A), the fibers are three-dimensionally arranged in the organ like the ribs of an upside down umbrella, with distinct fibers running in parallel to each prong. We note that the fibers cannot be motoneurons innervating muscles: in mosquitoes, as in all ectognath insects, the pedicel and the flagellum are un-musculated, and antennal muscles are restricted to the scape (Fig. 1A) [15, 21]. Superimposing the antibody stainings onto the respective bright field-images further revealed that the puncta and fibers do not follow major tracheae (Fig. S1B), arguing against artifacts from tracheal autofluorescence. Microtrachea autofluorescence, if present, would be expected to be more diffuse and not punctate in tangential views, and probably generate fluorescence hotspots in cross-sections.

70 JO is composed of multicellular scolopidia, each comprising supporting cap and scolopale
71 cells as well as two to three bipolar, monodendritic JO neurons with ciliated dendritic outer
72 segments [13] (Fig. 1A). Within the organ, the dendrites of the neurons point centrally with
73 their outer segments connecting to the prongs, whereas the axons project in the opposite
74 direction, running peripherally of the somata along the organ (Fig. 1A). Counterstaining the
75 neurons with an anti-horseradish peroxidase (anti-HRP) antibody localized the rows of nc46-
76 immunoreactive puncta between JO neuron somata and cilia to the dendritic inner segments
77 (Fig. 1B). An equivalent staining, including rows of puncta as well as strong
78 immunoreactivity in the proximal JO region where the axons come together, was obtained
79 with the monoclonal antibody 3C11 that recognizes presynaptic Synapsin [22] (Fig. 1D). Both
80 nc46 and 3C11 also yielded punctate stainings in the female JO (Fig. S1C), and
81 counterstaining the actin-based scolopale rods, which support the dendritic outer segments,
82 confirmed that the immunoreactive puncta localize to the dendritic inner segments (Fig. 1D,
83 Fig. S1C). Because of this dendritic localization, the respective fibers are unlikely to be JO
84 neuron axons, which are confined to the exterior region of JO, peripherally of JO neuron
85 dendrites and their somata (Fig. 1A).

86 To directly test for synapses in JO, we analyzed ultrathin sections of male antennae with
87 electron microscopy (Fig. 2A). Transmission electron micrographs showed abundant synaptic
88 sites in the proximal JO region where JO neurons come together (Fig. 2A,B). Presynaptic
89 fibers, identified by a dense packing with electron-lucent synaptic vesicles, were intermingled
90 between –and made contacts with– JO neuron axons (Fig. 2B). Electron-dense presynaptic
91 active zone and postsynaptic specializations confirmed these contacts as synaptic sites (Fig.
92 2B), documenting peripheral synapses for the male JO. Electron microscopy also identified
93 fibers packed with large dense core vesicles and smaller electron-lucid vesicles near almost

every sectioned dendritic inner segment (Fig. 2A,C). The latter fibers were intermingled between the dendritic inner segments next to their ciliary rootlets (Fig. 2A,C) and, more distally, near the ciliary basal bodies (Fig. 2A,D) that demarcate the junction between dendritic inner and outer segments (Fig. 2A,D). Bulging into (Fig. 2D, upper panels) –and passing through (Fig. 2D, lower panels)– the supporting scolopale cells, the fibers closely approached the dendrite membrane. Direct fiber-dendrite contacts or electron-dense synaptic specializations, however, could not be observed (Fig. 2D), pointing to a non-synaptic mode of vesicle release as known, for example, from modulatory octopaminergic neurons innervating insect muscles [23].

Hints on a central origin of the innervating fibers were obtained when we injected the neural tracer dextran-biotin into the pedicel of the antenna. Besides staining JO neurons, we co-labelled fibers in JO together with a somata cluster in the brain (Fig. 3A). Golgi impregnations of somata in the brain also co-stained fibers projecting up into the pedicel (Fig. 3B), further indicating a central JO innervation. Additional evidence for a central origin of the fibers was obtained when we tested for octopaminergic and serotonergic immunoreactivity in pedicellar sections. Anti-octopamine antibody labelled rows of puncta running along JO neuron dendrites (Fig. 3C), whereas cell bodies only displayed un-specific staining. Anti-serotonin antibody likewise failed to label somata within JO, yet it also recognized rows of puncta running along JO neuron dendrites (Fig. 3C). This anti-serotonin staining in JO is consistent with a previous report [24], which also failed to detect anti-serotonin-positive cell bodies in JO, but identified labelled fibers running through JO, along with one fiber projecting up in the flagellum (Fig.3D). In principle, the absence of stained somata in JO could reflect a local transmitter synthesis within the fibers, and at least some of the fibers could originate locally in JO. Invertebrate octopamineric and serotonergic neurons, however, usually all seem

118 to have somata inside the CNS, the only reported exception being a cell in the gut of an
119 earthworm species that seems part of the worm's peripheral nervous system [25-27]. In the
120 mosquito JO, the anti-serotonin-positive puncta could be traced down to the brain (Fig. 3E),
121 further documenting that the respective fibers connect to the CNS and that, rather than
122 harboring peripheral aminergic neurons, JO receives efferent CNS innervation.

123 Neither anti-serotonin nor anti-octopamine labelled the proximal JO region where the axons
124 come together, although this region harbors synapses (Fig. 2B) and displays presynaptic
125 marker staining (Fig. 1B,D). Staining of this region was also observed when we labeled
126 antennal sections with an anti-GAD antibody (Fig. 3C), which recognizes glutamic acid
127 decarboxylase (GAD) that converts glutamate into the neurotransmitter γ-aminobutyric acid
128 (GABA) [28]. Apparently, fibers innervating JO neuron axons and dendrites use different
129 neurotransmitters/neuromodulators, which might explain their different, synaptic and non-
130 synaptic innervation (Fig. 2).

131 To gain insights into putative efferent effects, we used a pharmacological approach and tested
132 whether octopamine impacts on JO function. Because auditory efferents reportedly modulate
133 cochlear mechanics in mammals by affecting outer hair cell motility [1-3], we analyzed the
134 mechanics of the male antennal flagellum whose vibrations are mechanically amplified by
135 motile JO neurons [15]. Flagellar mechanics were probed by monitoring flagellar vibrations
136 in response to sound and mechanical free fluctuations that arise from thermal bombardment
137 and JO neuron motility [15,29]. Following previous protocols [15,30-32], about 0.5 μl
138 solution containing 1mM octopamine dissolved in physiological saline [33] was administered
139 via thoracic injection. Treating eight control males with saline only did not alter their flagellar
140 mechanics: before treatment, the flagellar resonance frequency was 367 ± 24 Hz (mean ±
141 SD), consistent with a previous report [17]. Five minutes after treatment, the resonance

142 frequency was not significantly altered (349 ± 24 Hz, $p > 0.05$, two-tailed paired t-test), nor
143 was the maximum mechanical sensitivity of the flagellum (ratio between the spectral
144 vibration velocity and the corresponding particle velocity at the flagellar resonance, 6.2 ± 0.9
145 (ms^{-1}/ ms^{-1}) (before) *vs*. 5.7 ± 0.6 (ms^{-1}/ ms^{-1}) (after), $p > 0.05$). Also the power of the
146 mechanical free fluctuations of the flagellum in the absence of sound stimuli remained un-
147 changed upon saline injection (total power in the frequency band between 100 and 3,200 Hz,
148 $1.2 \cdot 10^3 \pm 2.7 \cdot 10^3$ nm^2 (before) *vs*. $2.7 \cdot 10^3 \pm 3.7 \cdot 10^3$ nm^2 (after), $p > 0.05$) (Fig. 4A,B),
149 documenting that JO neuron motility is not influenced by saline. Upon addition of
150 octopamine, however, the flagellar resonance frequency robustly shifted up from 370 ± 10 Hz
151 to 538 ± 38 Hz ($N = 8$, $p < 0.05$), which corresponds to approximately half an octave. This
152 alteration in frequency tuning associated with an increased maximum flagellar sensitivity (6.4
153 ± 1.7 (ms^{-1}/ ms^{-1}) (before) *vs*. 8.2 ± 2.4 (ms^{-1}/ ms^{-1}) (after), $p < 0.05$) and fluctuation power
154 ($0.5 \cdot 10^3 \pm 0.1 \cdot 10^3$ nm^2 (before) *vs*. $3.8 \cdot 10^3 \pm 3.9 \cdot 10^3$ nm^2 (after), $p < 0.05$), reporting
155 enhanced JO neuron motility and excess mechanical amplification [15, 33]. This excess
156 amplification associated with self-sustained feedback oscillations of the flagellum, giving rise
157 to sharp peaks in frequency spectra of its mechanical free fluctuations (Fig. 4A). Collectively,
158 these octopamine effects persisted when muscle activity was blocked by co-injecting 10 mM
159 glutamate [15] (Fig. S3), and equivalent effects were observed when we replaced octopamine
160 with the octopamine receptor agonist clonidine (1 mM) [34,35] (Fig. 4A,B). Treating animals
161 with the octopamine antagonist phentolamine (1 mM) [34,35] fully reverted the octopamine-
162 induced upward-shift of the flagellar resonance, shifting it back from 516 ± 49 Hz to 358 ± 29
163 Hz ($N = 8$, $p < 0.05$), close to the initial resonance frequency observed before octopamine
164 injection (384 ± 19Hz) (Fig. 4A,B). This restoration of the initial resonance, which documents
165 specificity and reversibility, was accompanied by a restoration of the initial flagellar

166 sensitivity, though in some animals the flagellum continued to oscillate self-sustained, and the
167 fluctuation power stayed increased (Fig. 4A,B).

168 Alterations in flagellar frequency tuning also ensued from the application of picrotoxin (1
169 mM), which blocks GABA receptors [36]. In line with previous observations [37], picrotoxin
170 was only effective when co-applied with collagenase, which itself left flagellar mechanics
171 unaffected (Fig. S2). Picrotoxin/collagenase, in addition to modulating flagellar sensitivity
172 and frequency tuning, strongly affected sound-evoked extracellular JO field potentials (Fig.
173 4C), which, analogous to cochlear potentials [38], display an oscillatory (AC) and a negative
174 sustained (DC) component [39] (Figs. 4C, S3B). Neither the AC nor the DC components were
175 affected by octopamine (Figs. 4C and S3B), and both components also remained unaltered
176 when collagenase was applied alone (Fig. S3A). Picrotoxin/collagenase, however, strongly
177 enhanced the DC component (Figs. 4C and S3B) – an effect that, in toadfish semicircular
178 canals, has been observed upon efferent stimulation [40,41].

179 We have presented evidence for an auditory efferent system in mosquitoes. Precedence for an
180 efferent innervation of arthropod mechanosensory organs comes from spiders [42-46] and
181 crustacean species [44,46], but the only hexapod mechanosensory organ that was previously
182 reported to receive efferent innervation is a locust hind leg proprioceptor [47]. Judging from
183 our results, the auditory efferent system of mosquitoes shares multiple parallels with its
184 vertebrate counterparts [1-3], including the targeting of auditory sensory cells and afferents
185 (Figs. 1,2), the use of several neurotransmitters/neuromodulators (Fig. 3), and the modulation
186 of mechanical and electrical sound responses (Fig. 4). The enhancement of the DC potentials
187 by picrotoxin (Fig. 4C) might reflect switch between coding strategies; the DC potentials have
188 been implicated in the ability of mosquitoes to detect –and to inter-individually synchronize–
189 high frequency harmonics of their wing-beat sounds [39], yet more work seems needed to

190 assess the biological significance of both these potentials and their modulation. Mosquito
191 mating behavior reportedly involves sophisticated acoustic interactions, including the
192 matching of flight-tone harmonics [17,39,48,49] and dynamic alterations of hearing organ
193 function [16]. Efferent modulation might enable male mosquitoes to dynamically lock onto –
194 and follow– the changing flight tones of females, which, judging from synaptic marker
195 stainings (Fig. S1C), also might use efferents for modulating auditory JO function [50]. Males
196 of some mosquito species also structurally modulate their flagellum, erecting the flagellar
197 hairs at dusks but collapsing them during the day via a turgor mechanism [51]. Also this
198 flagellar hair erection seems under CNS control and is susceptible to picrotoxin and
199 octopamine [52], indicating that efferents might control both JO function and the sound-
200 receiving properties of the flagellum. *Culex* lacks the ability to collapse its flagellar hairs [48],
201 yet its flagellum nonetheless receives serotonergic innervation (Fig. 3D) [24]. This suggests
202 that mosquitoes might extensively use efferents for modulating sensory neurons, including JO
203 neurons and, possibly, olfactory receptors in the antennal flagellum.

204

205 **Author Contributions**

206 M.A. and M.C.G. conceived the project. M.A. performed stainings, tracings, and electron
207 microscopy together with L.W., M.W., and S.P.. M.S., C.S., B.W, D.G., and M.C.G. analyzed
208 auditory effects, and M.A. and M.C.G. wrote the manuscript.

209 **Conflict of Interest**

210 The authors declare that they have no conflicts of interest.

211 **Acknowledgements**

212 We thank Jörg Egger and Melanie Nolden, Bayer CropBioscience, for providing the
213 experimental animals, the Develpmental Hybridoma Bank for antibodies, Maike Kittelmann

and Carolin Wichmann for help with electron microscopy, and Bart Geurten, Heribert Gras, Ralf Heinrich, and Andreas Stumpner for discussions. This work was supported by the International Max Planck Research School Neurosciences, Göttingen (to L.W.) and the German Science Foundation (DFG, GO 1092/4-1, SPP 1608, GO 1092/2-3, SFB 889 A1, and INST 186/1081-1) to M.C.G.

References

[1] Guinan JJ., Jr. (2010). Cochlear efferent innervation and function. Curr. Opin. Otolaryngol. Head Neck Surg. *18*, 447–453.

[2] Ryugo, D.K., Fay, R.R., and Popper, A.N. (2011). Auditory and vestibular efferents. Springer Handbook of Auditory Research *Vol. 38*, (Berlin: Springer).

[3] Sienknecht, U.J., Köppl, C., and Fritzsch, B. (2014). Evolution and development of hair cell polarity and efferent function in the inner ear. Brain Behav. Evol. *83*, 150–161.

[4] Field, L.H., and Matheson, T. (1998). Chordotonal organs of insects. Adv. Insect Physiol. *27*, 1–228.

[5] MacDermid, V., and Fullard, J. (1998). Not all receptor cells are equal: octopamine exerts no influence on auditory thresholds in the noctuid moth *Catocala cerogama*. Naturwissenschaften *85*, 505–507.

[6] Kamikouchi, A., Albert, J.T., and Göpfert, M.C. (2010). Mechanical feedback amplification in *Drosophila* hearing is independent of synaptic transmission. Eur. J. Neurosci. *31*, 697–703.

[7] Göpfert M.C., and Hennig, R.M. (2016). Hearing in insects. Ann. Rev. Entomol. *61*, 257–276.

[8] Roth, L. M. (1948). A study of mosquito behaviour. An experimental laboratory study of the sexual behavior of *Aedes aegypti* (Linnaeus). Am. Midl. Nat. *40*, 265–352.

[9] Tischner, H. and Schieff, A. (1955). Fluggeräusch und Schallwahrnehmung bei *Aedes aegypti* L. (Culicidae). Zool. Anz. *18* (Suppl.), 453–460.

242 [10] Clements, A.N. (1999). The antennae and hearing. In The Biology of Mosquitoes,
243 Clements, A.N. (New York: CABI Publishing), pp. 55–87.

244 [11] Howell, P.I., and Knols, B.G. (2009). Male mating biology. Malar. J. *8*, Suppl 2, S8.

245 [12] Johnston, C. (1855). Auditory apparatus of the *Culex* mosquito. Q. J. Microsc. Sci. *3*, 97–
246 102.

247 [13] Boo, K.S., and Richards, A.G. (1975). Fine structure of the scolopidia in the Johnston's
248 organ of male *Aedes aegypti* (L.) (Diptera: Culicidae). Int. J. Insect Morphol. Embryol. *4*,
249 549–566.

250 [14] Nadrowski, B., Effertz, T., Senthilan, P.R., and Göpfert, M.C. (2011). Antennal hearing
251 in insects – new findings, new questions. Hear. Res. *273*, 7–13.

252 [15] Göpfert, M.C., and Robert, D. (2001). Active auditory mechanics in mosquitoes. Proc.
253 Biol. Sci. *268*, 333–339.

254 [16] Jackson, J.C., and Robert, D. (2006). Nonlinear auditory mechanism enhances female
255 sounds for male mosquitoes. Proc. Natl. Acad. Sci. USA *103*, 16734–16739.

256 [17] Warren, B., Gibson, G., and Russell, I.J. (2009). Sex recognition through midflight
257 mating duets in *Culex* mosquitoes is mediated by acoustic distortion. Curr. Biol. *19*, 485–491.

258 [18] Belton, P. (1989). The structure and probable function of the internal cuticular parts of
259 Johnston's organ in mosquitoes (*Aedes aegypti*). Can. J. Zool. *67*, 2625–2632.

260 [19] Ignell, R., Dekker, T., Ghaninia, M., and Hansson, B.S. (2005). Neuronal architecture of
261 the mosquito deutocerebrum. J. Comp. Neurol. *493*, 207–240.

[20] Reichmuth, C., Becker, S., Benz, M., Debel, K., Reisch, D., Heimbeck, G., Hofbauer, A., Klagges, B., Pflugfelder, G.O., and Buchner, E. (1995). The *sap47* gene of *Drosophila melanogaster* codes for a novel conserved neuronal protein associated with synaptic terminals. Mol. Brain. Res. *32*, 45–54.

[21] Kristensen, N. P. (1981). Phylogeny of insect orders. Annu. Rev. Entomol. *26*, 135–157.

[22] Klagges, B.R., Heimbeck, G., Godenschwege, T.A., Hofbauer, A., Pflugfelder, G.O., Reifegerste, R., Reisch, D., Schaupp, M., Buchner, S., and Buchner, E. (1996). Invertebrate synapsins: a single gene codes for several isoforms in *Drosophila*. J. Neurosci. *16*, 3154–3165.

[23] Hoyle, G., Colquhoun, W., and Williams, M. (1980). Fine structure of an octopaminergic neuron and its terminals. J. Neurobiol. *11*, 103–126.

[24] Siju, K.P., B.S. Hansson, and Ignell, R. (2008). Immunocytochemical localization of serotonin in the central and peripheral chemosensory system of mosquitoes. Arthropod Struct. Dev. *37*, 248–259.

[25] Csoknya, M., et al. (1997). Octopamine-containing neurons in the alimentary tract of the earthworm (*Eisenia fetida*). Brain Res. 778, 414–417.

[26] Pflüger, H.J., and Stevenson, P.A. (2005). Evolutionary aspects of octopaminergic systems with emphasis on arthropods. Arthropod Struct. Dev. *34*, 379–396.

[27] Gillette, R. (2006). Evolution and function in serotonergic systems. Integr. Comp. Biol. *46*, 838–846.

[28] Roberts, E., and Frankel, S. (1950). gamma-aminobutyric acid in brain: its formation from glutamic acid. J. Biol. Chem. *187*, 55–63.

284 [29] Göpfert, M.C., Humphris, A.D., Albert, J.T., Robert, D., and Hendrich, O. (2005). Power
285 gain exhibited by motile mechanosensory neurons in *Drosophila* ears. Proc. Natl. Acad. Sci.
286 USA *102*, 325–330.

287 [30] Nesterov, A., Spalthoff, C., Kandasamy, R., Katana, R., Rankl, N.B., Andrés, M., Jähde,
288 P., Dorsch, J.A., Stam, L.F., Braun, F.J., Warren, B., Salgado, V.L., and Göpfert, M.C.
289 (2015). TRP channels in insect stretch receptors as insecticide targets. Neuron *86*, 665–671.

290 [31] Blau, C., and Wegener, G. (1994). Metabolic integration in locust flight: the effect of
291 octopamine on fructose 2,6-bisphosphate content of flight muscle in vivo. J. Comp. Physiol. B
292 *164*, 11–15.

293 [32] Stevenson, PA, Dyakonova V, Rillich J, and Schildberger K. (2005). Octopamine and
294 experience-dependent modulation of aggression in crickets. J. Neurosci. *25*, 1431–1441.

295 [33] Hayes, R. (1953). Determination of a physiological saline solution for *Aedes aegypti*
296 (L.). J. Econ. Entomol. *46*, 624–626.

297 [34] Evans, P.D. (1981). Multiple receptor types for octopamine in the locust. J. Physiol. *318*,
298 99–122.

299 [35] Kastner, K.W., Shoue, D.A., Estiu, G.L., Wolford, J., Fuerst, M.F., Markley, L.D.,
300 Izaguirre, J.A., and McDowell, M.A. (2014). Characterization of the *Anopheles gambiae*
301 octopamine receptor and discovery of potential agonists and antagonists using a combined
302 computational-experimental approach. Malar. J. *13*, 434.

303 [36] Sattelle, D.B., Lummis, S.C.R., Wong, J.F.H., and Rauh, J.J. (1991). Pharmacology of
304 insect GABA receptors. Neurochem. Res. *16*, 363–374.

305 [37] Stumpner, A. (1998). Picrotoxin eliminates frequency selectivity of an auditory
306 interneuron in a bushcricket. J. Neurophysiol. *79*, 2408–2415.

307 [38] Dallos, P. (1972).Cochlear potentials. A status report. Audiology *11*, 29–41.

308 [39] Cator, L.J., Arthur, B.J., Harrington, L.C., and Hoy, R.R. (2009). Harmonic convergence
309 in the love songs of the dengue vector mosquito. Science *323*, 1077–1079.

310 [40] Highstein, S.M., and Baker, R. (1985). Action of the efferent vestibular system on
311 primary afferents in the toadfish, *Opsanus tau*. J. Neurophysiol. *54*, 370–84.

312 [41] McCue, M.P., and Guinan, J.J. Jr. (1994). Influence of efferent stimulation on
313 acoustically responsive vestibular afferents in the cat. J. Neurosci. *14*, 6071–6083.

314 [42] Foelix, R.F. (1975). Occurrence of synapses in peripheral sensory nerves of arachnids.
315 Nature *254*, 146–148.

316 [43] Fabian-Fine, R., Meinertzhagen, I.A., and Seyfarth, E.-A. (2000). Organization of
317 efferent peripheral synapses at mechanosensory neurons in spiders. J. Comp. Neurol. *420*,
318 195–210.

319 [44] Fabian-Fine, R., Seyfarth, E.-A., and Meinertzhagen, I.A. (2002). Peripheral synaptic
320 contacts at mechanoreceptors in arachnids and crustaceans: morphological and
321 immunocytochemical characteristics. Microsc. Res. Tech. *58*, 283–298.

322 [45] Widmer, A., Höger, U., Meisner, S., French, A.S., and Torkkeli, P.H. (2005). Spider
323 peripheral mechanosensory neurons are directly innervated and modulated by octopaminergic
324 efferents. J. Neurosci. *25*, 1588–1598.

325 [46] Cattaert, D., Le Bon, M., and Le Ray, D. (2002). Efferent controls in crustacean
326 mechanoreceptors. Microsc. Res. Tech. *58*, 312–324.

[47] Bräunig, P., and Eder, M. (1998). Locust dorsal unpaired median (DUM) neurons directly innervate and modulate hindleg proprioceptors. J. Exp. Biol. *201*, 3333–3338.

[48] Gibson, G, Warren, B., and Russell, I.J. (2010). Humming in tune: sex and species recognition by mosquitoes on the wing. J. Assoc. Res. Otolaryngol. *11*, 527-540.

[49] Simões, P.M., Ingham, R.A., Gibson, G. & Russell, I.J. (2016). A role for acoustic distortion in novel rapid frequency modulation behaviour in free-flying male mosquitoes. J. Exp. Biol., in press (doi: 10.1242/jeb.135293).

[50] Göpfert, M.C., and Robert, D. (2000). Nanometre-range acoustic sensitivity in male and female mosquitoes. Proc Biol Sci. *267*, 453–457.

[51] Nijhout, H.F., and Sheffield, H.G. (1979) Antennal hair erection in male mosquitoes: a new mechanical effector in insects. Science *20*, 595–596.

[52] Nijhout, H.F (1977). Control of antennal hair erection in male mosquitoes. Biol. Bull. *153*, 591–603.

[53] Avitabile, D., Homer, M., Champneys, A.R., Jackson, J.C., and Robert, D. (2010). Mathematical modelling of the active hearing process in mosquitoes. J. R. Soc. Interface *7*,105–122.

344 ## Figure legends

345 **Figure 1.** Presynaptic marker staining in the male JO. (**A**) Sketches of JO (left) and a single
346 JO scolopidium (right) with two neurons and supporting cap (CC) and scolopale (SC) cells.
347 Ax: axons; D: dendrites; DI: dendritic inner segments; DO: ciliated dendritic outer segments;
348 SO: somata. Modified from [13,53]. (**B-D**) Presynaptic marker staining. JO neurons are
349 counterstained with the neuronal marker anti-HRP (red). (**B**) nc46. Left: overview, showing
350 nc46-positive puncta running between JO neuron dendrites and somata (arrows) and nc46
351 staining the proximal JO region where JO neuron axons come together (asterisks). Middle:
352 zoom-ins of the puncta (top, arrows) and the latter axonal region (bottom, asterisks). Right:
353 Respective staining from another individual. (**C**) Close-up of nc46-positive puncta, showing
354 nc46-positive fibers between puncta (arrows). (**D**). 3C11 staining. The actin-based rods that
355 surround the dendritic outer segments are counterstained with phalloidin (blue). Left:
356 overview. M: muscles. Right: close-up of 3C11-positive puncta at the dendritic inner
357 segments. Asterisks and arrows as in B.

358 **Figure 2.** Synaptic and non-synaptic release sites in JO. (**A**) Top: ultrathin section through a
359 male pedicel highlighting the zoom-in regions of panels B to D. Bottom: sketch of the
360 junction between JO neuron dendritic inner and outer segments, with proximal (pB) and distal
361 (dB) basal bodies, ciliary rootlets (Rt), and ciliary axoneme. (**B**) Presynaptic fibers
362 (highlighted in blue) synapse onto JO neuron axons (AX). Top, left: overview. Top right:
363 zoom-in, depicting two fibers and synaptic contact sites (arrowheads). Bottom: zoom-ins of
364 single synapses. SV: synaptic vesicles. Arrowheads: electron-dense post- and presynaptic
365 (possibly T-bars) specializations. (**C**) Fiber terminals at JO neuron inner dendritic segments.
366 Top: overview, highlighting several fibers (blue) intermingled between inner dendritic
367 segments next to the ciliary rootlets. Bottom: zoom-ins of the fibers, showing electron-dense

368 (DV) and -lucid (LV) vesicles. (**D**) Fiber terminals next to JO neuron basal bodies. Left:
369 overviews. Right: respective zoom-ins, depicting vesicles.

370 **Figure 3**. Fiber origins and neurotransmitters. (**A**). Dextran-biotin staining of fibers in JO co-
371 stains somata in the brain. Left: bright-field image, depicting tracheae. Right: Superimposed
372 dextran-biotin staining, showing fibers (pink circle) and somata (yellow circle), in addition to
373 tracheal auto-fluorescence. (**B**) Golgi staining of somata in the anterior-lateral brain region
374 (yellow arrows) co-stains fibers (white arrows) projecting in the pedicel (pink arrow). Right:
375 zoom-in from (B), depicting the proximal edge of the pedicel (arrowheads) and entering fibers
376 (pink arrows). (**C**) Anti-octopamine (left), -GAD (middle), and -serotonin (right) antibody
377 stainings. Neurons are counterstained with anti-HRP (red). Anti-octopamine and –serotonin
378 recognize puncta (arrows) running between JO neurons somata (SO) and dendrites (D). Anti-
379 GAD recognizes the proximal JO region where the axons join (asterisks). (**D**) Anti-serotonin-
380 positive puncta (arrows) in the flagellum. Inset: same puncta, without anti-HRP and bright-
381 field. (**E**) Anti-serotonin-positive puncta (arrows) in JO project to the brain (left: overview,
382 right, zoom-in).

383

384 **Figure 4**. Octopamine and GABA effects on auditory organ function. (**A**) Frequency spectra
385 (lin-log) of the mechanical sound responses (top) and free fluctuations (bottom) of male
386 flagella before and after injections (N = 8 males each, whereby each line represents the
387 spectrum of one male antenna). Amplitudes of sound responses (top) are given as the flagellar
388 vibration velocity v_{vib} (m/s) normalized to the sound particle velocity u (m/s), and spectral
389 amplitudes of the flagellar free fluctuations are presented in nm/Hz. For additional data, see
390 Fig. S2. (**B**) Respective flagellar resonance frequencies (top) and maximum mechanical
391 sensitivities (middle) of the flagellar sound responses and corresponding fluctuation powers

392 (bottom) determined by integrating the power spectra for frequencies between 100 and 3,200
393 Hz. *: significant difference ($p < 0.05$, two-tailed paired t-tests). (**C**) Tone-evoked (stimulus,
394 top) JO field potentials (responses, bottom) before and after octopamine (left) or
395 picrotoxin/collagenase (right) injection (examples from 3 animals each). Injecting
396 picrotoxin/collagenase, but not octopamine or collagenase alone (Fig. S3A), enhances the DC
397 potential component (see also Fig. S3B).

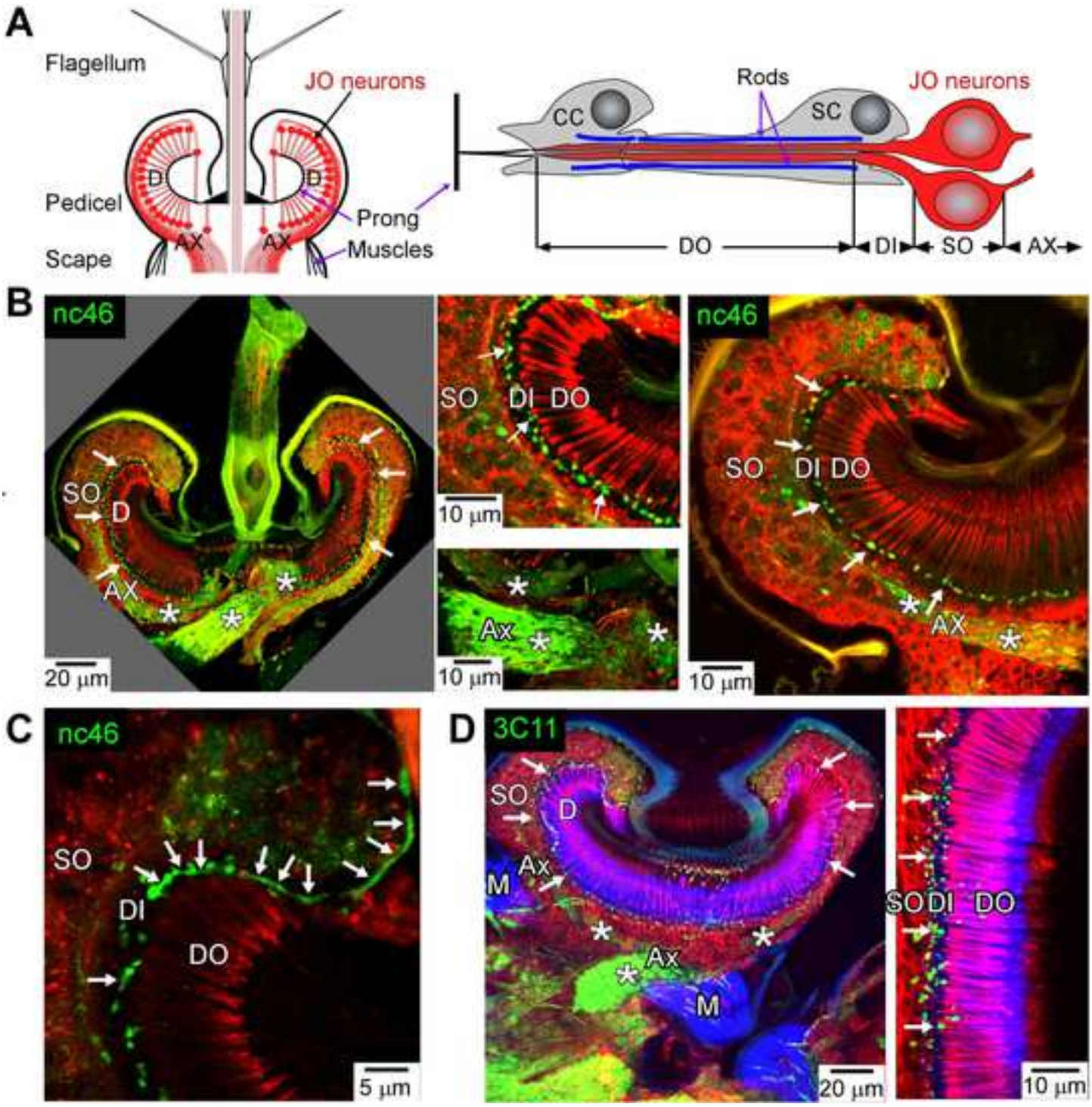
A
Flagellum
JO neurons
Pedicel
Scape
D
D
AX
AX
Prong
Muscles
Rods
CC
SC
JO neurons
DO
DI
SO
AX
B
nc46
SO
D
AX
20 µm
SO
DI
DO
10 µm
Ax
10 µm
nc46
SO
DI
DO
AX
10 µm
C
nc46
SO
DI
DO
5 µm
D
3C11
SO
D
Ax
M
Ax
M
20 µm
SO
DI
DO
10 µm

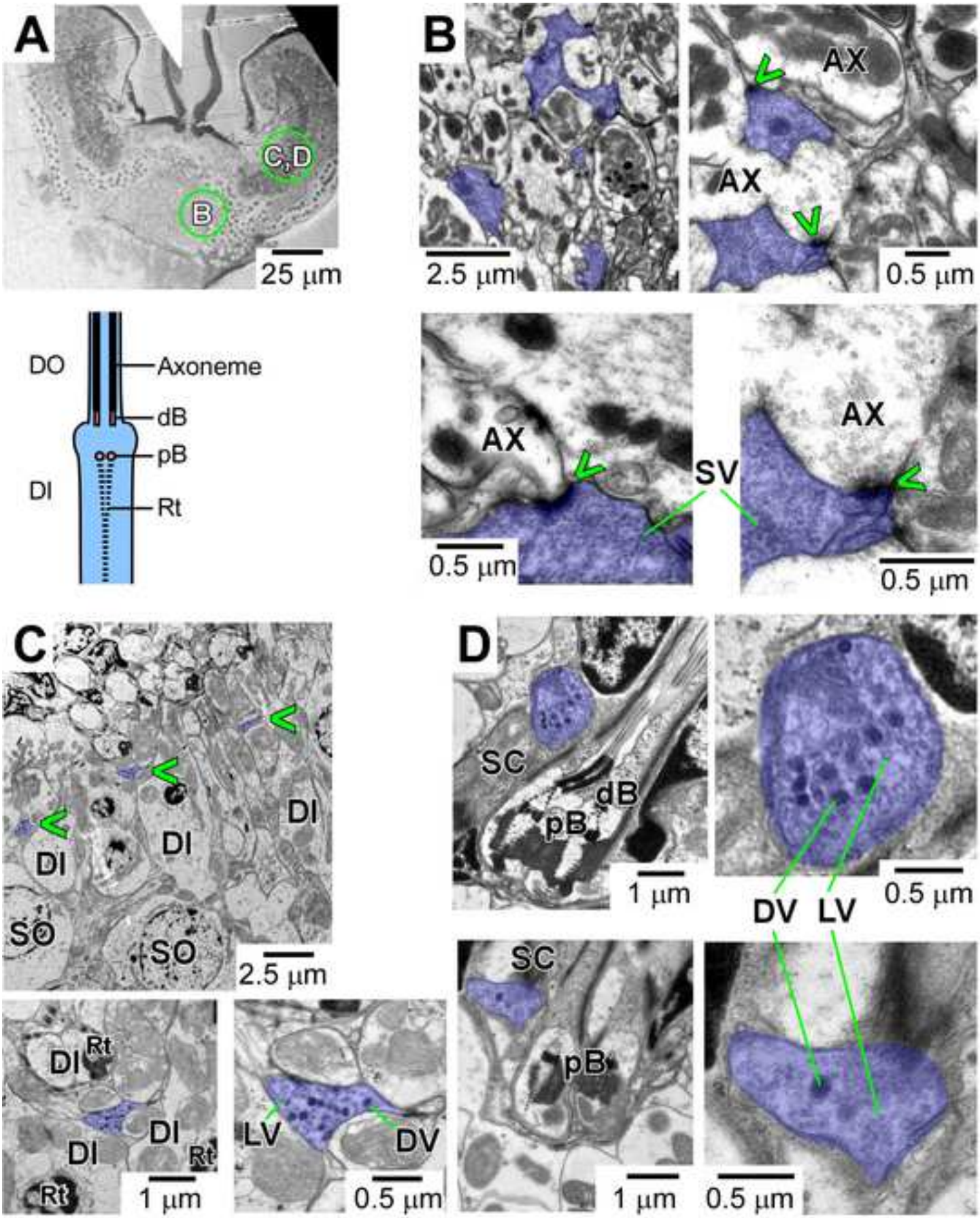
A
C, D
B
25 µm
DO
Axoneme
dB
pB
DI
Rt
B
2.5 µm
AX
AX
0.5 µm
AX
SV
0.5 µm
AX
0.5 µm
C
DI
DI
DI
SO
SO
2.5 µm
DI
Rt
DI
DI
Rt
Rt
1 µm
LV
DV
0.5 µm
D
SC
dB
pB
1 µm
DV
LV
0.5 µm
SC
pB
1 µm
0.5 µm

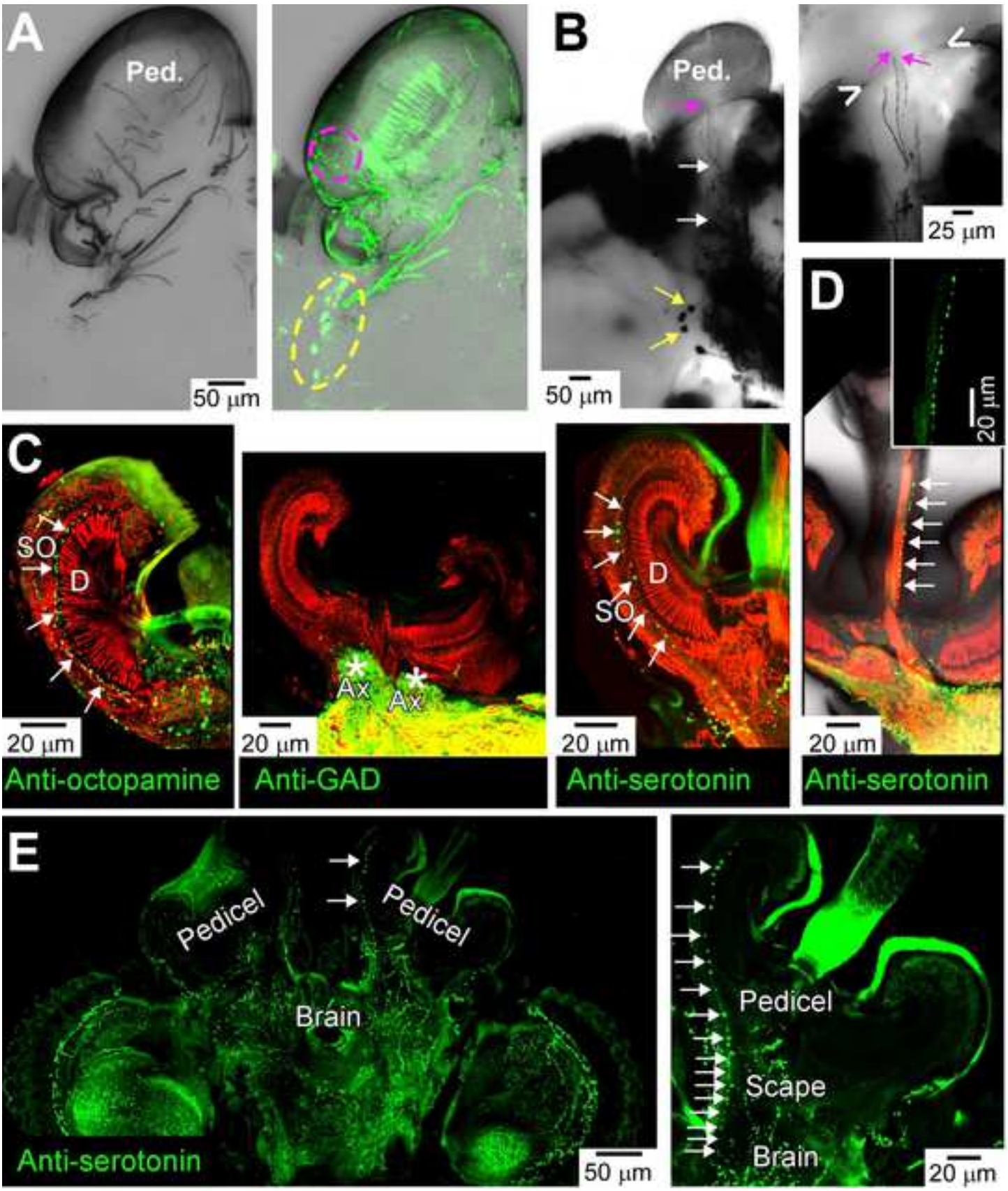
A
Ped.
50 μm
B
Ped.
50 μm
25 μm
C
SO
D
20 μm
Anti-octopamine
Ax
Ax
20 μm
Anti-GAD
D
SO
20 μm
Anti-serotonin
D
20 μm
20 μm
Anti-serotonin
E
Pedicel
Pedicel
Brain
Anti-serotonin
50 μm
Pedicel
Scape
Brain
20 μm

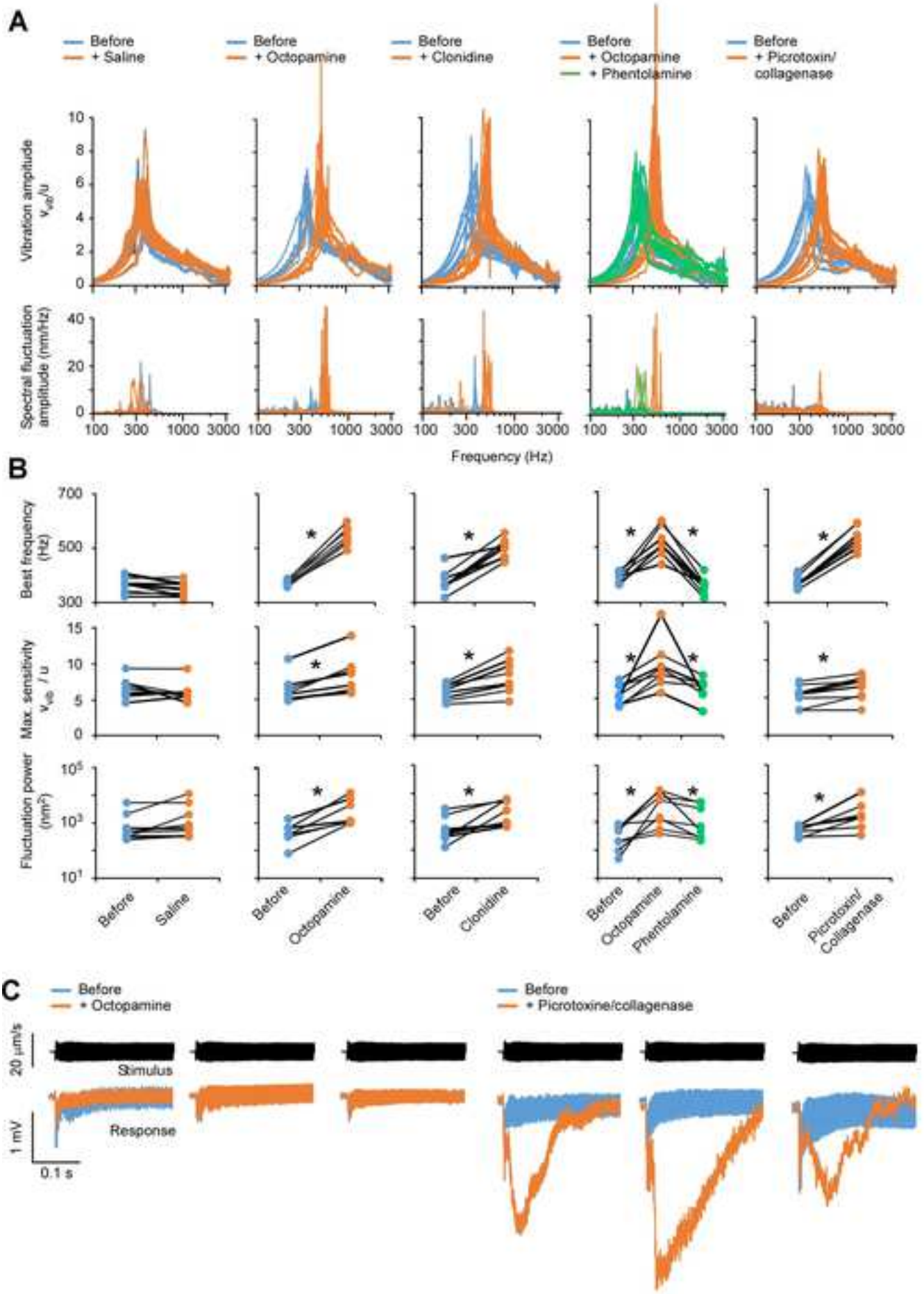
A
Before
+ Saline
Before
+ Octopamine
Before
+ Clonidine
Before
+ Octopamine
+ Phentolamine
Before
+ Picrotoxin/
collagenase
Vibration amplitude
Spectral fluctuation amplitude (nm/Hz)
Frequency (Hz)
B
Best frequency (Hz)
Max. sensitivity
Fluctuation power (nm²)
Before
Saline
Before
Octopamine
Before
Clonidine
Before
Octopamine
Phentolamine
Before
Picrotoxin/
Collagenase
C
Before
+ Octopamine
Before
+ Picrotoxine/collagenase
20 µm/s
Stimulus
Response
1 mV
0.1 s

Inventory of supplemental materials

Supplemental Information includes three figures (associated with Figs. 1 and 4) and supplemental experimental procedures.

Supplemental Information

Auditory Efferent System controls Mosquito Hearing

Marta Andrés, Marvin Seifert, Christian Spalthoff, Ben Warren, Lukas Weiss, Diego Giraldo, Margret Winkler, Stephanie Pauls, and Martin C. Göpfert

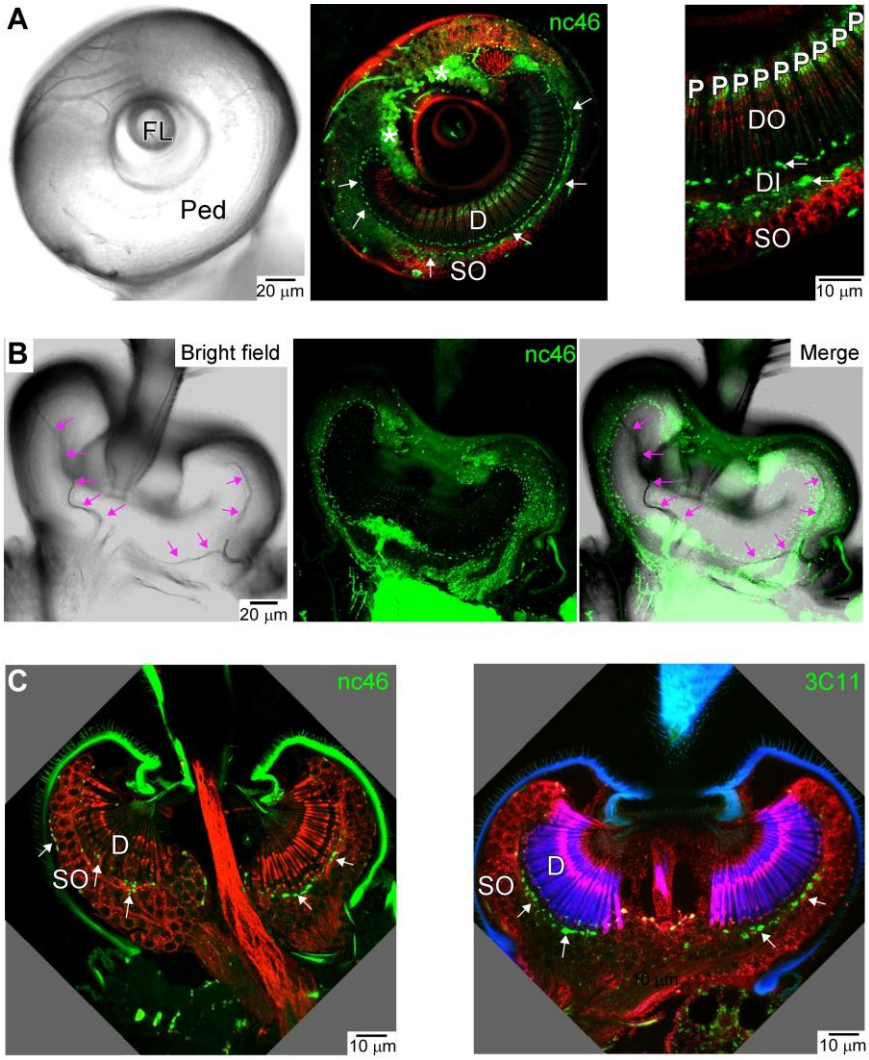

Figure S1, associated with Fig. 1. (**A**) Oblique section through the pedicel stained with nc46 (green) and anti-HRP (red) antibodies. Left: bright field image (FL: antennal flagellum; Ped: antennal pedicel). Middle: respective antibody signals, depicting rows of nc46 puncta running peripherally through the organ (arrows) and staining in the proximal JO region (asterisks). Right: zoom-in. SO: somata; DI: dendrites, DO: dendritic outer segments; DI: dendritic inner segments; P: prongs (visible through cuticular autofluorescence). Note that several puncta occur peripherally of each prong. (**B**) nc46 signals are not caused by tracheal auto-fluorescence. Left: bright field image, highlighting tracheae in JO (pink arrows). Middle: respective nc46 antibody staining. Right: merge, documenting that nc46 signals do not follow tracheae. (**C**) Presynaptic markers yield punctate staining in the JO of female *Culex quinquefasciatus*. Left, green: nc46 antibody staining. Right, green: 3C11 antibody staining. Neurons are counterstained with anti-HRP antibody (red) and, in the right panel, the actin-based rods that surround the ciliated dendritic outer segments of JO neurons are stained with phalloidin (blue). White arrows highlight the punctate staining running along JO neurons, between dendrites (D) and somata (SO).

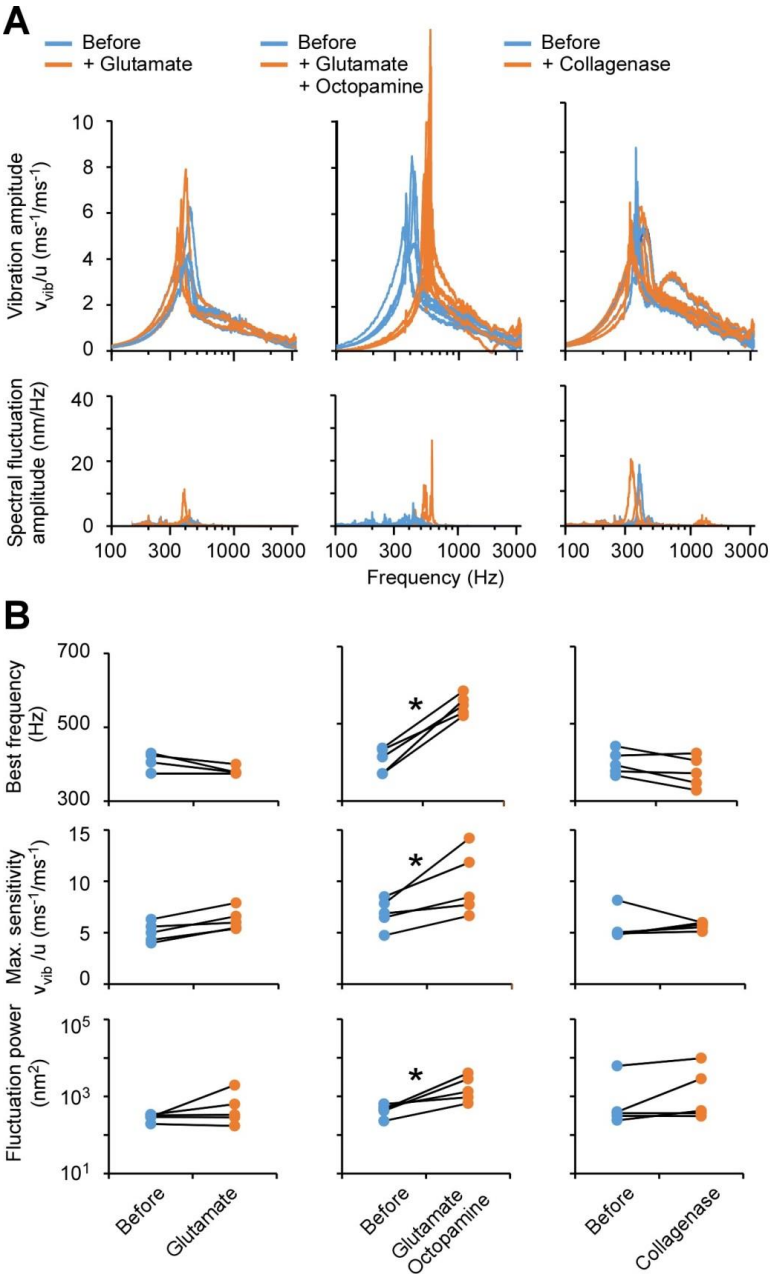

Figure S2, associated with Fig. 4A,B. (**A**) Frequency spectra (lin-log) of the mechanical sound responses (top) and free fluctuations (bottom) of the antennal flagellum before and after thoracic injection of glutamate (left), which blocks muscles, glutamate and octopamine together (middle), and collagenase (right). For details, see legend to Fig. 4A. (**B**) Respective resonance frequencies (top), maximum sensitivities (middle) and fluctuation powers (bottom). *: significant ($p < 0.05$, N = 5 animals each, sign tests). For additional details, see legends to Fig. 4A,B.

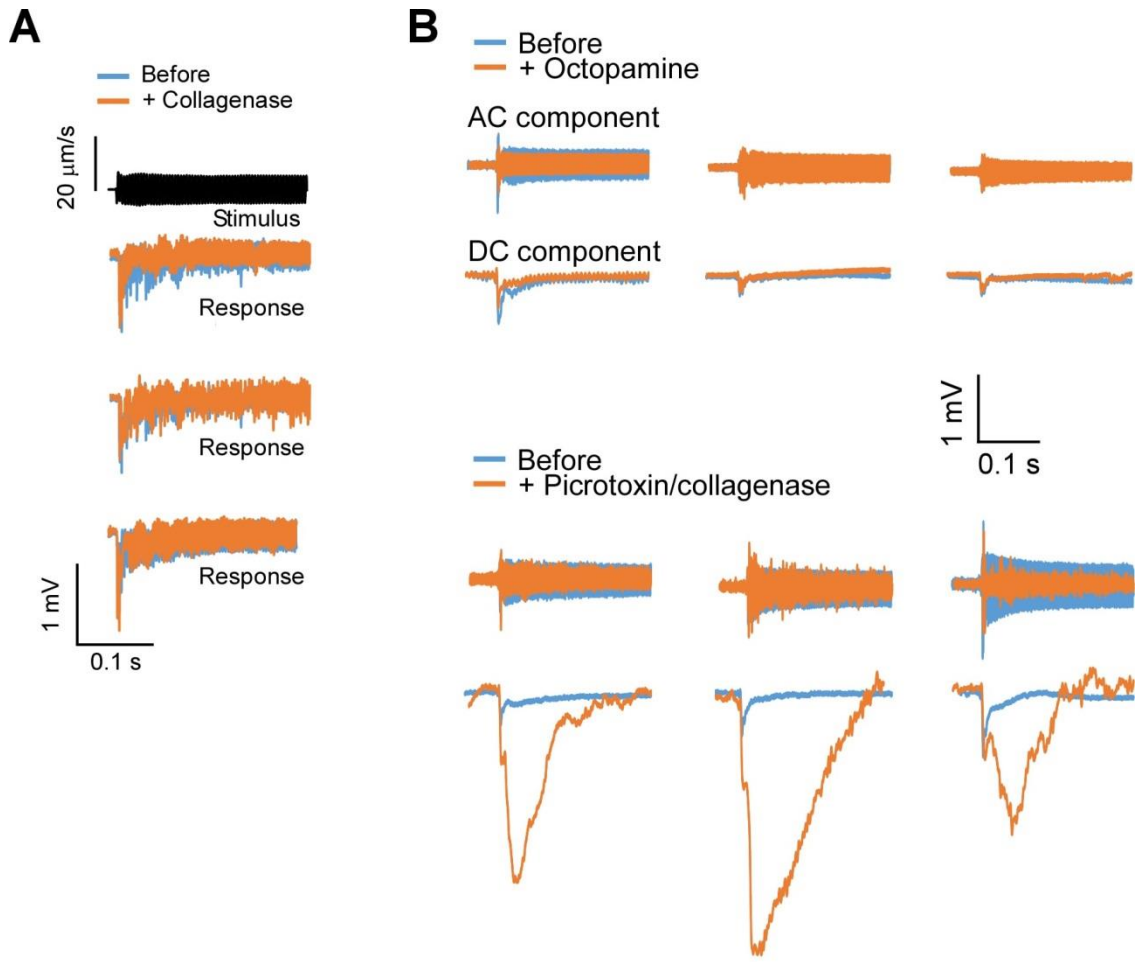

Figure S3, associated with Fig. 4C. Effects of octopamine and picrotoxin/collagenase on sound-evoked antennal nerve field potentials. (**A**) Collagenase alone does not affect the potentials. (**B**) AC and DC components of the sound-evoked potentials in Fig. 4C isolated by digital high- (AC component) and low-pass (DC component) filtering (230 Hz corner frequency). For additional details, see legend to Fig. C.

Supplemental Experimental Procedures

Experimental animals

Culex quinquefasciatus mosquito eggs were kindly provided by Bayer CropBioscience (Monheim am Rhein, Germany). Eggs were placed in aquarium water until pupariation. Pupae were collected in glass bowls and placed in square cages (20 x 20 x 20 cm) for hatching. Mosquitoes were kept at 25°C temperature and 60% humidity, with a photoperiod of 12:12 h light/dark. Adults were given constant access to cotton pads soaked with a 10% sucrose solution. For experiments, 3-day-old imagines were used.

Immunohistochemistry

Upon removal of the proboscis, mosquito heads were fixed in 4% paraformaldehyde for 3-4 hours at 4°C. After fixation, heads were embedded in albumin/gelatin and post-fixed in 6% formaldehyde overnight at 4°C. Vibratome sections (40 µm) of post-fixed heads were made in 0.01 M phosphate-buffered saline (PBS, pH 7.4). Sections were washed in PBS with 0.3% TritonX-100 (PBST), and non-specific binding sites were blocked with a blocking solution containing 5% normal goat serum (NGS) and 2% bovine serum albumin (BSA) in PBS with 1% TritonX-100. Sections were incubated with primary antibodies diluted in the blocking solution overnight at 4°C. Primary antibodies were: mAb nc46 (anti-SAP47), mAb 3C11 (anti-Synapsin), (both 1:50; Developmental Studies Hybridoma Bank, University of Iowa, http://dshb.biology.uiowa.edu/), anti-HRP (1:500; Sigma-Aldrich, St. Louis, Missouri, USA), rabbit anti-serotonin (1:500; Sigma-Aldrich), and rabbit anti-glutamic acid decarboxylase (anti-GAD, 1:1000; Sigma Aldrich). Upon washing with PBST, sections were incubated with the secondary antibodies diluted in blocking solution at room temperature for 1 hour. Corresponding Alexa Fluor Dyes (1:500; Thermo Fisher) and Alexa Fluor Phalloidin 633 (1:50; Thermo Fisher) were used as secondary antibodies. After further washes in PBST and PBS, sections were mounted in DABCO (Sigma-Aldrich) and analyzed with a Leica TCS SP8 confocal microscope (Leica Microsystems GmbH, Wetzlar, Germany).

For anti-octopamine staining, heads were fixed in 0.1M sodium cacodylate, 2% paraformaldehyde and 1% glutaraldehyde in phosphate buffer (pH 7.4) for 3-4 hours at 4°C. Heads were embedded in albumin/gelatin and post-fixed in 6% formaldehyde overnight at 4°C. Vibratome sections were made in 0.05M Tris buffer containing 0.85% sodium metabisulfite (Tris-SMB). Sections were incubated for 10 minutes in Tris-SMB containing 0.1M sodium borohydride and washed in Tris-SMB. Sections were additionally washed overnight at 4°C in Tris-SMB containing 30% saccharose. After some further washes in Tris-SMB, sections were treated with a blocking solution consisting of 1% normal goat serum, 0.25% BSA, and 3% milk powder in Tris-SMB containing 0.25% TritonX-100. Samples were incubated with primary mouse anti-octopamine antibody (1:1000; Jena Bioscience GmbH, Jena, Germany, http://www.jenabioscience.com/) and rabbit anti-HRP antibody (1:500; Sigma-Aldrich) dissolved in the blocking solution for 2 to 3 days at 4°C.

Electron microscopy

Heads were fixed in a solution containing 2% paraformaldehyde and 2.5% glutaraldehyde in 0.05M sodium cacodylate buffer (pH 7.4) overnight at 4°C [Ref. S1]. Heads were then washed in 0.05M sodium cacodylate buffer and treated with 2% osmium tetroxide for 1.5

hours at 4°C. Afterwards, they were transferred to phosphate buffer (pH 7.4) and dehydrated in ascending ethanol concentrations until 70%. At this point, heads were counterstained with uranyl acetate in 70% ethanol for 30 minutes and finally dehydrated in 100% ethanol. Samples were immersed twice in propylene oxide for 10 minutes, taken through ascending propylene oxide: Durcupan solutions (1 hour in 3: 1; overnight in 1:1 and 1 hour in 1:3), embedded in Durcupan, and allowed to polymerize for 48 hours at 65°C. 50-70 nm ultrathin sections were cut with a Leica/Reichert Ultracut E Ultramicrotome (Leica Microsystems, Wetzlar, Germany), collected on 50 mesh hexagonal copper grids and contrasted with uranyl acetate (30 min) and lead citrate (2 min) [Ref. S2] and examined with a Zeiss EM 902 B transmission electron microscope (Carl Zeiss AG, Oberkochen, Germany).

Neuronal tracings

To trace the auditory efferent neurons, the neuronal tracer dextran-biotin 3000 MW (Molecular Probes) was pressure injected into the pedicel of tethered mosquitoes. The following steps were performed mostly in the dark. Mosquitoes were kept 6 hours at room temperature in a humidity chamber to allow for retrograde transport. Upon decapitation and removal of the proboscis, heads were fixed in 4% paraformaldehyde for 1 hour, embedded in albumin/gelatin and post-fixed in 6% formaldehyde overnight at 4°C. For visualizations, 30 µm vibratome sections were treated with the conjugated antibodies Streptavidin Alexa Fluor 488 (1:500; Thermo Scientific, Waltham, USA) and anti-HRP-Cy3 (1:300; Jackson ImmunoResearch, Baltimore, USA), washed with PBST and PBS, and finally mounted in DABCO (Sigma Aldrich).

Golgi staining

Golgi impregnation was performed as described [19]. Mosquitoes were immersed in cold 2.5% potassium dichromate containing 3 g sucrose/100 ml. Animals were decapitated and the distal parts of the proboscis and the antennal flagella were removed. Heads were transferred to a 2.5% dichromate solution with 25% glutaraldehyde (5:1) containing 1.3 g sucrose/ 100ml for 5 days at 4°C. Heads were washed several times in cold 2.5% potassium dichromate and transferred to 2.5% potassium dichromate with 1% osmium tetroxide (99:1) where they were kept at 4°C for 4 days in darkness. Heads were then briefly washed in dH_2O and transferred to a series of 0.75% silver nitrate baths until no more precipitate appeared from the tissue and heads were kept in this solution in the dark for 3 days at 4° C. Subsequently, heads were briefly washed in dH_2O, dehydrated in ascending alcohol concentrations and immersed in propylene oxide for 10 minutes before embedding them in a 1:1 mixture of propylene oxide and Durcupan plastic (Fluka, Heidelberg, Germany). After 24 hours under the fume hood to allow the propylene oxide to evaporate, fresh Durcupan was added and the preparations were polymerized at 65 ºC for 48 hours. Preparations were sectioned horizontally at 20 µm.

Auditory organ function

Methods of thoracic compound administration have been described [15,25]. In brief, a hole was punched into the thorax using a micropipette and a drop of the solution (ca. 0.5 µl) was put on top. Intake of the drop ensued automatically from the low pressure of the body, which sucked in the drop. All compounds tested were obtained from Sigma Aldrich. The

respective solutions were set up at least 1 h prior to the experiments and stored at room temperature (21°C-23°C), excluding possible ectothermic effects that might take place while setting up the solutions. In control experiments, in which we heated up the solutions to 70°C and monitored their temperature with a miniature thermistor, they fully equilibrated to room temperature in the injection pipette within one minute. This equilibration time is shorter than the time it took us to start the injections, which means that even if the starting solutions would have been hot (or cold), they would have assumed room temperature at the time of their injection.

To assess auditory organ function, mechanical free fluctuations and sound-induced vibrations of the tip of the antennal flagellum were monitored with a Polytec PSV-400 laser Doppler vibrometer (Polytec GmbH, Waldbronn, Germany) [15,43] (see also Ref. S3). For acoustic stimulation, we used sound chirps (frequency-modulated sweeps) with a sound particle velocity amplitude of approximately 5 μm/s and a linear frequency increase from 1 to 3,200 Hz within one second. Sound-evoked field potentials were recorded via an electrolytically tapered tungsten electrode inserted into the joint between head and antenna, with the indifferent electrode placed in the thorax [15,43]. Potentials were measured in response to 320 Hz tones with a sound particle velocity amplitude of approximately 5 μm/s and a duration of 1.2 s. Sound stimuli were generated with Polytec signal generator software, power amplified, and fed to a loud speaker placed 7 cm behind the animal. The resulting sound particle velocity was monitored with an EM Emkay NR 3158 pressure gradient microphone (distributed by Knowles Electronics Inc., Itasca, USA) placed besides the animal (for microphone calibration, see Ref. S2). Signals were conditioned with antialiasing filters and digitized at a rate of 8.192 kHz by using an Analogic 16 Fast A/D board. To compute frequency spectra, time windows, 1 s in length (rectangular windowing function) were subjected to Fast Fourier transforms (FFTs), whereby ca. 20 (sound responses) or ca. 100 (free fluctuations) FFTs were averaged to determine the Fourier amplitudes of the laser and microphone signals (Ref. S2). The potential responses shown in Figs. 4C and S3 represent averages of 10 repetitions.

Supplementary references

S1 Dacks, A.M., Christensen, T.A., Agricola, H.J., Wollweber, L., and Hildebrand, J.G. (2005). Octopamine-immunoreactive neurons in the brain and subesophageal ganglion of the hawkmoth *Manduca sexta*. J. Comp. Neurol. *488*, 255–268.

S2 Reynolds, E.S. (1963). The use of lead citrate at high pH as an electron-opaque stain in electron microscopy. J. Cell Biol. *17*, 208–212.

S3 Albert, J. T., Nadrowski, B., Kamikouchi, A. , and Göpfert, M. C. (2006). Mechanical tracing of protein function in the *Drosophila* ear. Nat. Protoc, doi:10.1038/nprot.2006.364